Communication

Effect of Microstructure on Molecular Oxygen Permeation through Condensed Phospholipid Monolayers

Gang Pu, Marjorie L. Longo, and Mark A. Borden

J. Am. Chem. Soc., **2005**, 127 (18), 6524-6525• DOI: 10.1021/ja051103q • Publication Date (Web): 15 April 2005

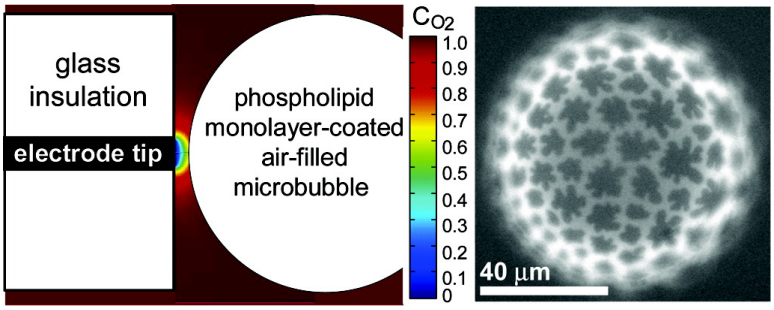

More About This Article

Additional resources and features associated with this article are available within the HTML version:

- Supporting Information
- Links to the 2 articles that cite this article, as of the time of this article download
- Access to high resolution figures
- Links to articles and content related to this article
- Copyright permission to reproduce figures and/or text from this article

View the Full Text HTML

J|A|C|S
COMMUNICATIONS

Published on Web 04/15/2005

Effect of Microstructure on Molecular Oxygen Permeation through Condensed Phospholipid Monolayers

Gang Pu,[†] Marjorie L. Longo,*[,†] and Mark A. Borden*[,‡]

Department of Chemical Engineering & Materials Science and Department of Biomedical Engineering, University of California, Davis, California 95616

Received February 21, 2005; E-mail: mllongo@ucdavis.edu; maborden@ucdavis.edu

The oxygen permeability of phospholipid monolayers at the air−water interface is important for the gas exchange function of biological monolayers[1] and the stability of natural and synthetic microbubbles.[2] The lipid monolayer shell of a stable microbubble is in the unique state of being fully condensed, in which the tension in the interface is negligible[3] and the gas permeability is very low.[4,5] Fluorescence microscopy results have shown phase coexistence in the monolayer shell consisting of crystalline domains separated by disordered phase boundaries.[6] We recently developed a novel technique that utilizes a microelectrode in the induced transfer mode[7] to measure the oxygen permeability of the microbubble shell.[5] Herein, we report on a study that combined these two techniques to correlate oxygen permeability measurements to known microstructure for the first time in phospholipid monolayers.

Microbubbles were formed by sonification of an aqueous surfactant mixture in the presence of air. The shell materials consisted of a homologous series of saturated diacyl phosphatidylcholine lipids (C16, C18, C20, C22, and C24). Fluorescence microscopy allowed visualization of the microstructure of newly formed microbubbles. Dark crystalline domains were easily visualized within the probe-rich disordered phase (Figure 1). Control of shell microstructure was performed by heating the microbubble suspension above the lipid main phase transition temperature and then cooling at different rates, including slow (1−2 °C/min), medium (15−35 °C/min), and rapid (100−700 °C/min). Average domain perimeter (L) and area (A) were measured for each lipid acyl chain length and cooling rate. Average domain size decreased exponentially with increasing cooling rate and was independent of chain length. Domain shape, however, depended on *both* cooling rate and acyl chain length, as illustrated in Figure 1. The domain boundary density ($\beta = L/A$; boundary length per unit area) was obtained for each shell composition at each cooling rate. Heat-treated microbubbles were incubated at room temperature for 2 h to allow the shell to fully compress such that the condensed phase domains were closely packed, area fraction of the disordered phase was minimized, and surface tension in the shell was negligible.[3,5,6]

Oxygen permeability was measured in a custom chamber on a microscope stage by positioning a microelectrode next to a microbubble held stationary with a micropipet (Figure 2). Oxygen transfer from the bubble was induced by maintaining a potential of −0.5 V at the electrode tip that resulted in diffusion-limited oxygen consumption and the development of a steady-state concentration gradient. Steady-state current−distance profiles were obtained as the microbubble was incrementally translated toward the stationary electrode. We developed a FEMLAB package to model oxygen transport through the lipid monolayer shell and intervening aqueous medium; results from these simulations verified earlier assumptions of negligible effects of curvature and gas core shrinkage.[5] A typical steady-state concentration profile is superimposed onto the schematic setup in Figure 2 to illustrate the concentration gradient during dissolved oxygen transport from the microbubble gas core to the electrode tip. Normalized steady-state current intensity versus separation distance was determined by integrating the oxygen flux over the electrode surface. The oxygen permeability of the monolayer shell was determined by comparing FEMLAB simulations to the experimentally determined steady-state current−distance profile.

Figure 3 shows a plot of the experimentally determined oxygen permeability as a function of the domain boundary density.

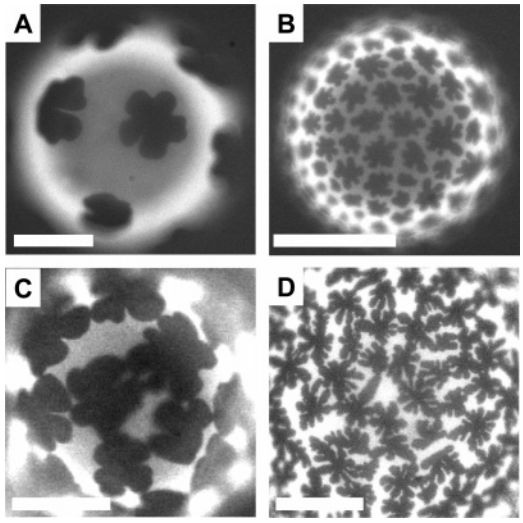

Figure 1. Fluorescent micrographs of heat-treated microbubble shells showing shape of dark condensed phase domains surrounded by bright disordered phase region: (a,b) C18, (c,d) C24; (a,c) slow cooling, (b,d) rapid cooling. Scale bars represent 40 μm.

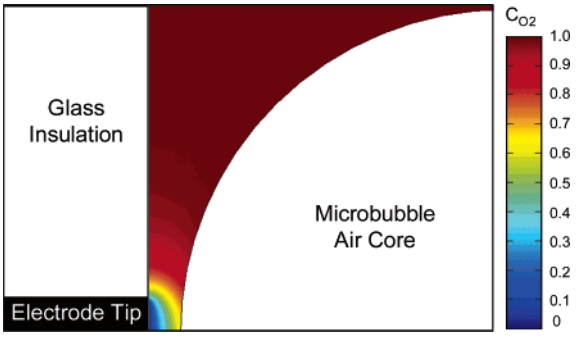

Figure 2. Surface plot showing normalized oxygen concentration profile (color scale shown on right) for the electrode−bubble setup (P = 0.001 cm/s; $d/a = 1.0$ where d is the bubble−electrode separation distance and a is the electrode tip radius). Consumption at the charged electrode tip induces oxygen transfer from the bubble air core.

[†] Department of Chemical Engineering & Materials Science.
[‡] Department of Biomedical Engineering.

10.1021/ja051103q CCC: $30.25

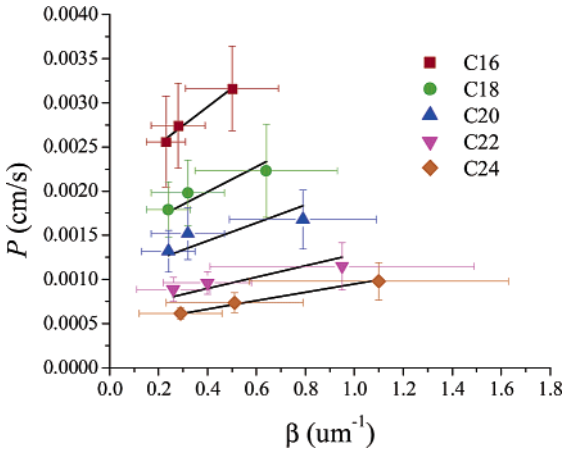

Figure 3. Oxygen permeability of the monolayer shell as a function of the domain boundary density for each phospholipid acyl chain length. Error bars include standard deviations of resistance, domain area, and domain perimeter measurements; lines are linear least-squares fits of eq 1 for each chain length. The permeability increases in proportion to the amount of accessible area available in the domain boundary regions.

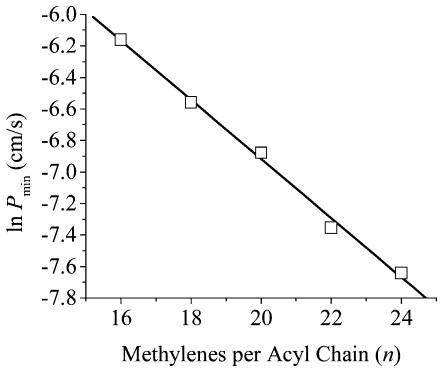

Figure 4. Minimum permeability at $\beta = 0$ (□) versus acyl chain length. The increase in activation energy per additional methylene group was calculated from the slope of the linear trendline.

Permeability decreased significantly as chain length increased for a given microstructure. For each lipid, oxygen permeability increased linearly with domain boundary density, indicating that permeation occurs readily through the accessible area of the disordered interdomain regions. Furthermore, permeability decreased exponentially with increasing lipid acyl chain length (n) for a given domain boundary density (Figure 4), showing that lipid composition plays a crucial role in determining the oxygen transport rate through both the domain and boundary regions.

The exponential relationship between P and n supports the energy barrier theory for monolayer penetration rather than the macroscopic continuum approach of solubility and Fick's diffusion, which would predict a linear relationship.[8−10] The energy barrier theory predicts a mechanism that is analogous to gas diffusion through interstitial sites in a crystalline lattice. The dependence of permeability on defect density indicates that poor packing at the domain boundaries facilitates such transport. G. T. Barnes noted that the shortcomings of conventional monolayer permeation theories, which attempt to calculate monolayer permeability a priori based on fundamental properties, likely arise because they do not account for microstructural effects.[11] Our results correlating permeability to microstructure clearly support this view. We propose the following modification to the energy barrier theory to account for the influence of domain boundaries:

$$P = (1 + \beta)\cdot\alpha \exp\left(\frac{-E_n n}{kT}\right) \quad (1)$$

where α is an empirical constant, E_n is the increase in activation energy per additional methylene group, k is Boltzmann's constant, and T is temperature. The minimum permeability (P_{min}), approximated for a single crystal, is given by eq 1 setting $\beta = 0$ and is shown as a function of chain length in Figure 4. The value of E_n was calculated from the slope of the linear trendline to be 110 cal/mol, in close agreement with previous results for gas permeation through insoluble monolayers.[5,9] Permeation through the single crystal would likely occur through intradomain defects (i.e., subdomain boundaries). The finite nature of the domains and their boundaries suggests that β will have a limiting maximum value and corresponding permeability that should also depend on acyl chain length. This model unifies the effects of composition and microstructure by combining the concepts of the accessible area theory, in terms of the domain boundary density, and energy barrier theory for monolayer permeation.

Electrodes have been used previously to measure the effects of composition and surface pressure on oxygen transport through lipid monolayers at the air−water interface.[12,13] Likewise, the exponential relationship between gas/vapor permeability and hydrocarbon chain length has been described previously.[8,9,12] In the current study, we utilized the unique properties of a lipid-coated microbubble, including a well-defined microstructure and fully condensed state of the shell, to measure for the first time the essential effects of domain boundary density on the oxygen transport rate through a phospholipid monolayer.

Acknowledgment. Funding was provided by the Office of Naval Research Hydromechanics Program (Grant N000140510002) and the Center for Polymeric Interfaces and Macromolecular Assemblies (Grant NSF DMR 0213618). We are very grateful to Joe and Essie Smith for endowing part of this work.

Supporting Information Available: Experimental details. Tabulated microstructural parameters. Experimental steady-state current−distance profiles. Details of FEMLAB simulation. This material is available free of charge via the Internet at http://pubs.acs.org.

References

(1) (a) Connor, L. M.; Ballinger, C. A.; Albrecht, T. B.; Postlethwait, E. M. *Am. J. Physiol.* **2004**, *286*, L1169−L1178. (b) Blank, M. *Gen. Physiol.* **1968**, *52*, 191S−208S.
(2) (a) Johnson, B. D.; Cooke, R. C. *Science* **1981**, *213*, 209−211. (b) Unger, E. C.; Porter, T.; Culp, W.; Labell, R.; Matsunaga, T.; Zutshi, R. *Adv. Drug Delivery Rev.* **2004**, *56*, 1291−1314.
(3) Duncan, P. B.; Needham, D. *Langmuir* **2004**, *20*, 2567−2578.
(4) Borden, M. A.; Longo, M. L. *Langmuir* **2002**, *18*, 9225−9233.
(5) Borden, M. A.; Longo, M. L. *J. Phys. Chem. B* **2004**, *108*, 6009−6016.
(6) (a) Kim, D. H.; Costello, M. J.; Duncan, P. B.; Needham, D. *Langmuir* **2003**, *19*, 8455−8466. (b) Borden, M. A.; Pu, G.; Runner, G. J.; Longo, M. L. *Colloids Surf., B* **2004**, *35*, 209−223.
(7) Barker, A. L.; Macpherson, J. V.; Slevin, C. J.; Unwin, P. R. *J. Phys. Chem. B* **1998**, *102*, 1586−1598.
(8) Langmuir, I.; Langmuir, D. *J. Phys. Chem.* **1927**, *31*, 1719−1731.
(9) La Mer, V. K. *Retardation of Evaporation by Monolayers*; Academic Press: New York, 1962; pp 59−66.
(10) Blank, M. *J. Phys. Chem.* **1962**, *66*, 1911−1918.
(11) Barnes, G. T. *Colloids Surf., A* **1997**, *126*, 149−158.
(12) Zhang, J.; Unwin, P. R. *Langmuir* **2002**, *18*, 1218−1224.
(13) Ciani, I.; Burt, D. P.; Daniele, S.; Unwin, P. R. *J. Phys. Chem. B* **2004**, *108*, 3801−3809.

JA051103Q